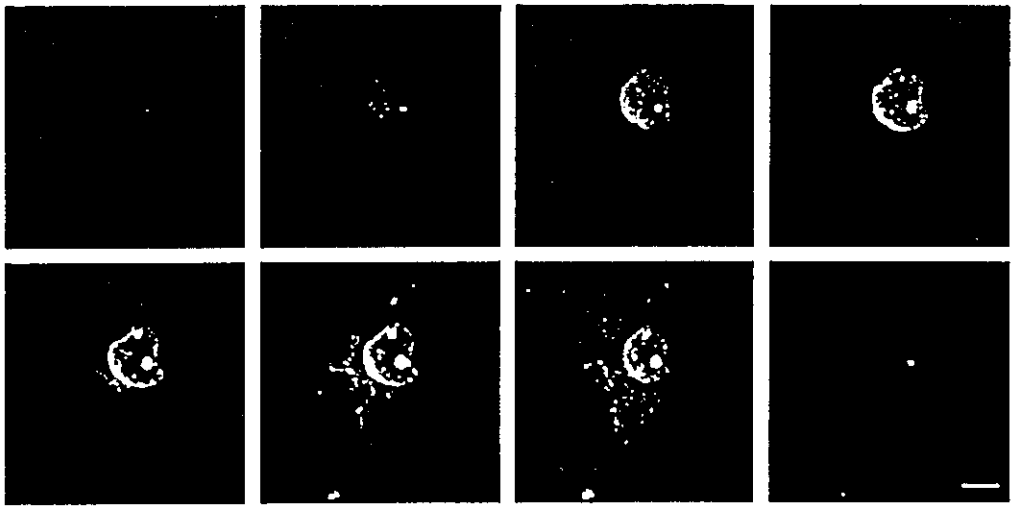

Fig. 4. R_{11}KC-conjugated QDs were accumulated in nucleous. Cells were stimulated by R_{11}KC-QD as described in Fig. 3. The cells were observed by confocal microscopy. The images are collected in the Z-direction at the span of 0.1 μm. Bars indicated 10 μm. Magnifications: ×120.

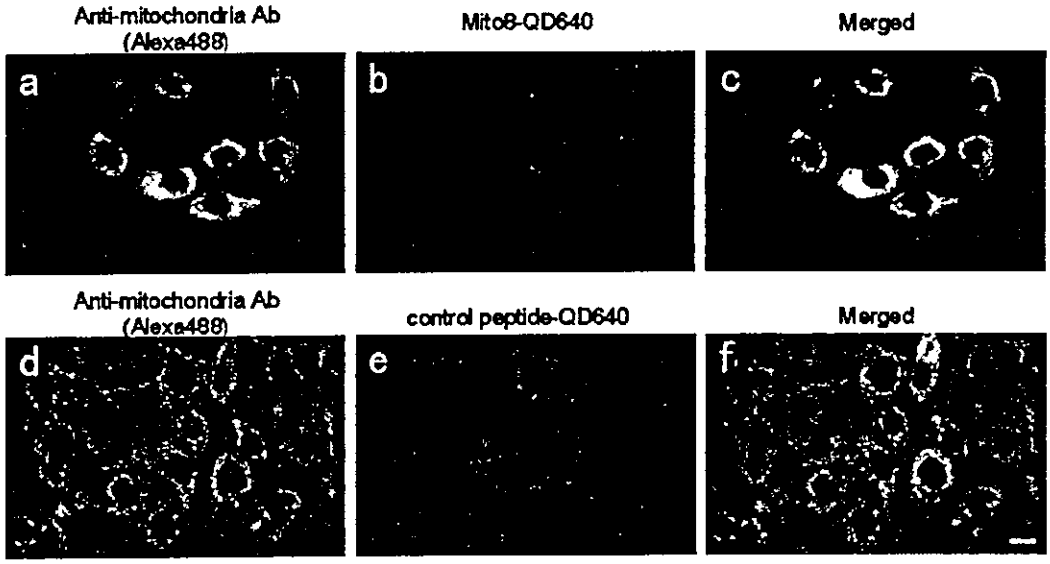

Fig. 5. Mitochondria images of Vero cells. Vero cells were stimulated with 1 μM with Mito-8 QD640 (a–c) or control START QD640 (d–f), and incubated for 12 hr under 37 C conditions. Cells were then fixed, and stained with anti-human mitochondria (M2) antibody. The cells were observed by fluorescent microscopy. Bars indicated 10 μm.

cence intensity enhanced remarkably after the secondary coupling with the target peptide (Fig. 2b). This result suggested that covering QD with the high molecular weight polymer such as polypeptides might prohibit the leakage of electron and might contribute to the continuative electron-rich condition of whole QD particle.

Next we evaluated whether the function of signal peptides would be held after conjugated with QDs. To confirm this, FITC-conjugated R_{11}KC peptides were conjugated with QD640 (fluorescence 640 nm, emitted red) and added to the cultured COS7 cells. We previously reported that QD without any peptides resulted in cellular-uptake into endosome by endocytotic pathways (17, 33). In this case, the red fluorescence from QD was located in nucleus and co-localized with that from FITC (Fig. 3a). This result indicated that QDs with nuclear peptides acquire another function that was based on R_{11}KC peptides. Unlabeled R_{11}KC remained in this study because the labeling efficiency of QDs with

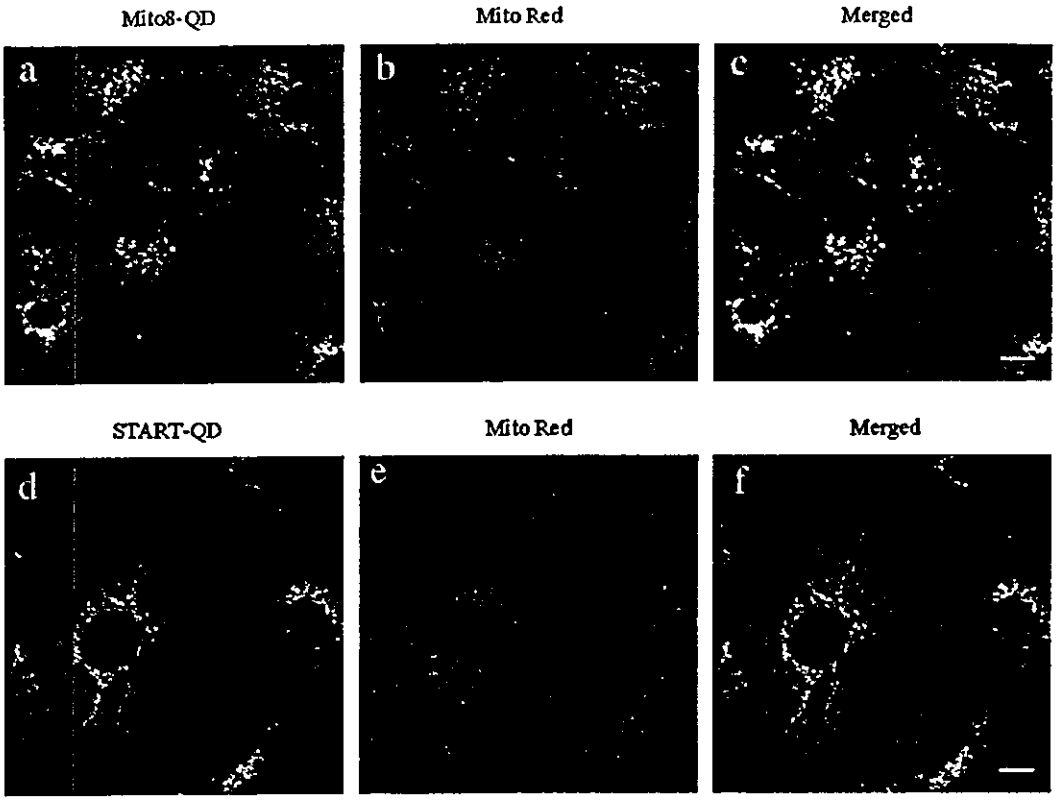

Fig. 6. Living mitochondria images by confocal microscope. Vero cells were cultured with 1 μM QD520-Mito8 (a–c) or QD520-START (control peptide, d–f) for 12 hr under 37 C conditions. Then cells were co-stimulated with MitoRed® mitochondria staining reagents (Dojindo Laboratories) for more additional 1 hr. After stimulation, cells were observed by confocal microscopy as shown in Fig. 4. Bars indicated 20 μm. Magnifications: ×80.

Fig. 7. Two kinds of signal peptide-QD showed independent behavior in the cells. Vero cells were co-stimulated with 1 μM QD640-Mito8 (emitted red) and QD-R_{11}KC (emitted green) for 12 hr under 37 C conditions. After fixed, the cells were observed by confocal microscopy. Bars indicated 20 μm.

oligopeptides was approximately 40% in this method and almost all of the FITC-tagged R_{11}KCs were not labeled with QDs. This result indicated that the R_{11}KC-QD has the same capability to localize into a nucleus as original ones. It is already reported that R_{11}KC peptide is rapidly localized into a nucleus by incubating for 10 min (25, 39). Then we tried to track the footmark of R_{11}KC peptide into nucleus in living cells for 15 min. Vero cells were treated with R_{11}KC-conjugated QD640 and continuously observed under a culture fluorescent microscopy (Fig. 3b). The penetration from the cell membrane to nuclei was observed about 30 sec after incubation, and precedently located into nucleus after 1 min. R_{11}KC-QDs were gradually accumulated the

whole nucleus during 15 min incubation. To investigate the localization of R_{11}KC-QDs into the nucleus, QDs distribution in the nucleus was observed by confocal microscopy (Fig. 4). R_{11}KC-QDs were dispersed in the whole nucleus and partially accumulated in nucleolus. In this study, we demonstrated that QDs as well as other fusion protein could also transit into nucleus with the help of nuclear signaling peptides.

Next we assessed the function of mitochondria signal peptides with QDs (Fig. 5). Mito-8 peptide- and control START peptide-coated QD640 (fluorescence 640 nm, emitted red) were incubated with cells and stained with anti-mitochondrial antibody. QD-red signal with Mito-8 gave raise to yellow in merged images (Fig. 5c). In contrast, red fluorescence emitted from control START peptides was not co-localized with that of mitochondria signal (Fig. 5f). Then we tried to visualize mitochondria distribution in living cells. Mito8-QD520 peptide was co-cultured with MitoRed® mitochondria staining dyes (Dojindo Laboratories, Japan). After incubation, the cells were observed by confocal laser microscopy (Fig. 6). QD-Mito-8 green luminescences from QD520 were also co-localized with conventional mitochondria probes. These results indicated that QDs with functional oligopeptides possessed dual functions to localize specific organelle and to emit high detectable fluorescence. Then we demonstrate the mixture of those two peptide separately move to their assigned organelle. The mixture of R_{11}KC-QD640 and Mito-8-QD520 were added to the Vero cells (Fig. 7). Red luminescence from R_{11}KC was separated from green ones from Mito-8 and not co-localized with each other, implying that QDs with functional peptides were individually transported to the target organelle.

Now several groups have reported that QDs conjugated with antibodies and some peptides for biological assays and cellular imaging *in vitro* and *in vivo* were demonstrated as brighter and longer lifetime probes (27–30). In this article, we demonstrated the various signal peptides conjugated with fluorescent QDs to both deliver QDs into living cells and selectively target specific organelles in living cells. In addition, these peptides-QD complexes have ability to translocate itself across the cell plasma membrane and can subsequently home to their specific targets such as the nucleus or the mitochondria. These results indicated that we succeeded in adding the new function as "information" to QDs by conjugating them with peptides. Our previous studies showed that QD-conjugated albumin and QD-glycerol can be targeted to the endosome and cytoplasm, respectively (14, 17). We showed in this article that QDs with targeted peptides can be also transported to nuclei and mitochondria. These techniques have the possibility that QDs can reveal transduction of proteins and peptides to specific subcellular compartments *in vitro* and even *in vivo* as a powerful tool for conducting intracellular analysis. We suggest that this technology could have a significant impact on the field of molecular and cellular biology as well as biotechnology. Recently, the plan that applied a novel nanomaterial such as nanocrystal QDs to the medical field attracted attention as one of the industrial applications of nanotechnology. And what is more, it is expected that QDs will be applied in the medical field for the innovative investigation, diagnosis and treatment of various diseases (8, 36, 38). It is very important to produce nanometer-sized materials with biological function, since we have no "designed material" which can arbitrarily penetrate nanometer-size gaps such as the skin, membrane, a blood vessel, and so on. This study demonstrates that these surface modifications of functional molecules combined with nanoparticles may work as bio-nanomachines conforming to the functions designated by their surface molecules. Nanomaterials have a great capacity of changing even the concept of existing diagnosis and medical treatment, by giving functions such as the pharmacological and magnetic effects, by giving the information of the specificity to tissue or organs *in vivo*. Novel nanomaterials including QD-supermolecules can be utilized as a transporter of the intracellular drug and gene delivery tools in the future.

We thank Mr. Kazuyuki Ito for valuable advice and help with proofreading. This work was supported by Medical Techniques Promotion Research Grant from the Ministry of Health, Labour and Welfare of Japan (H14-nano-004, Kenji Yamamoto).

References

1) Aglipay, J.A., Lee, S.W., Okada, S., Fujiuchi, N., Ohtsuka, T., Kwak, J.C., Wang, Y., Johnstone, R.W., Deng, C., Qin, J., and Ouchi, T. 2003. Oncogene **22**: 8931–8938.
2) Akerman, M.E., Chan, W.C., Laakkonen, P., Bhatia, S.N., and Ruoslahti, E. 2002. Nanocrystal targeting *in vivo*. Proc. Natl. Acad. Sci. U.S.A. **99**: 12617–12621.
3) Ballou, B., Lagerholm, B.C., Ernst, L.A., Bruchez, M.P., and Waggoner, A.S. 2004. Noninvasive imaging of quantum dots in mice. Bioconjugate Chem. **15**: 79–86.
4) Bruchez, M., Jr., Moronne, M., Gin, P., Weiss, S., and Alivisatos, A.P. 1998. Semiconductor nanocrystals as fluorescent biological labels. Science **281**: 2013–2016.
5) Chan, W.C., and Nie, S. 1998. Quantum dot bioconjugates for ultrasensitive nonisotopic detection. Science **281**: 2016–2018.
6) Dabboussi, B.O., Rodriguez-Viejo, J., Mikulec, F.V., Hein, J.R., Mattoussi, H., Ober, R., Jensen, K.F., and Bawendi, M.G. 1997. (CdSe)ZnS core-shell quantum dots; synthesis and characterization of size series of highly luminescent nanocrystallites. J. Phys. Chem. **101**: 9463–9475.

7) Dubertret, B., Skourides, P., Norris, D.J., Noireaux, V., Brivanlou, A.H., and Libchaber, A. 2002. *In vivo* imaging of quantum dots encapsulated in phospholipid micelles. Science **298**: 1759–1762.
8) Gao, X., Chan, W.C., and Nie, S. 2002. Quantum-dot nanocrystals for ultrasensitive biological labeling and multicolor optical encoding. J. Biomed. Opt. **7**: 532–537.
9) Gao, X., Cui, Y., Levenson, R.M., Chung, L.W.K., and Nie, S. 2004. *In vivo* cancer targeting and imaging with semiconductor quantum dots. Nat. Biotechnol. **22**: 969–976.
10) Gerion, D., Pinaud, F., Williams, S.C., Parak, W.J., Zanchet, D., Weiss, S., and Alivisatos, A.P. 2001. Synthesis and properties of biocompatible water-soluble silica-coated CdSe/ZnS semiconductor quantum dots. J. Phys. Chem. **105**: 8861–8871.
11) Goldman, E.R., Anderson, G.P., Tran, P.T., Mattoussi, H., Charles, P.T., and Mauro, J.M. 2002. Conjugation of luminescent quantum dots with antibodies using an engineered adaptor protein to provide new reagents for fluoroimmunoassays. Anal. Chem. **74**: 841–847.
12) Gorlich, D., and Mattaj, I.W. 1996. Nucleocytoplasmic transport. Science **271**: 1513–1518.
13) Haggie, P.M., and Verkman, A.S. 2002. Diffusion of tricarboxylic acid cycle enzymes in the mitochondrial matrix *in vivo*. Evidence for restricted mobility of a multienzyme complex. J. Biol. Chem. **277**: 40782–40788.
14) Hanaki, K., Momo, A., Oku, T., Komoto, A., Maenosono, S., Yamaguchi, Y., and Yamamoto, K. 2003. Semiconductor quantum dot/albumin complex is a long-life and highly photostable endosome marker. Biochem. Biophys. Res. Commun. **302**: 496–501.
15) Hines, M.A., and Guyot-Sionnest, P. 1996. Synthesis and characterization of strongly luminescing ZnS-capped CdSe nanocrystals. J. Phys. Chem. **100**: 468–471.
16) Hoshino, A., Fujioka, K., Oku, T., Suga, M., Sasaki, Y.F., Ohta, T., Yasuhara, M., Suzuki, K., and Yamamoto, K. 2004. Physicochemical properties and cellular toxicity of nanocrystal quantum dots depend on their surface modification. Nano Lett. **4**: 2163–2169.
17) Hoshino, A., Hanaki, K., Suzuki, K., and Yamamoto, K. 2004. The applications T-lymphoma labeled with fluorescent quantum dots to cell trafficking markers in a mouse body. Biochem. Biophys. Res. Commun. **314**: 46–53.
18) Ishii, D., Kinbara, K., Ishida, Y., Ishii, N., Okochi, M., Yohda, M., and Aida, T. 2003. Chaperonin-mediated stabilization and ATP-triggered release of semiconductor nanoparticles. Nature **423**: 628–632.
19) Jaiswal, J.K., Mattoussi, H., Mauro, J.M., and Simon, S.M. 2003. Long-term multiple color imaging of live cells using quantum dot bioconjugates. Nat. Biotechnol. **21**: 47–51.
20) Johnson, L.V., Walsh, M.L., and Chen, L.B. 1980. Localization of mitochondria in living cells with rhodamine 123. Proc. Natl. Acad. Sci. U.S.A. **77**: 990–994.
21) Kaether, C., and Gerdes, H.H. 1995. Visualization of protein transport along the secretory pathway using green fluorescent protein. FEBS Lett. **369**: 267–271.
22) Kaul, Z., Yaguchi, T., Kaul, S.C., Hirano, T., Wadhwa, R., and Taira, K. 2003. Mortalin imaging in normal and cancer cells with quantum dot immuno-conjugates. Cell Res. **13**: 503–507.
23) Larson, D.R., Zipfel, W.R., Williams, R.M., Clark, S.W., Bruchez, M.P., Wise, F.W., and Webb, W.W. 2003. Water-soluble quantum dots for multiphoton fluorescence imaging *in vivo*. Science **300**: 1434–1436.
24) Lidke, D.S., Nagy, P., Heintzmann, R., Arndt-Jovin, D.J., Post, J.N., Grecco, H.E., Jares-Erijman, E.A., and Jovin, T.M. 2004. Quantum dot ligands provide new insights into erbB/HER receptor-mediated signal transduction. Nat. Biotechnol. **22**: 198–203.
25) Matsushita, M., Tomizawa, K., Moriwaki, A., Li, S.T., Terada, H., and Matsui, H.J. 2001. A high-efficiency protein transduction system demonstrating the role of PKA in long-lasting long-term potentiation. J. Neurosci. **21**: 6000–6007.
26) Mattaj, I.W., and Englmeier, L. 1998. Nucleocytoplasmic transport: the soluble phase. Annu. Rev. Biochem. **67**: 265–306.
27) Mattoussi, H., Mauro, J.M., Goldman, E.R., Anderson, G.P., Sundar, V.C., Mikulec, F.V., and Bawendi, M.G. 2000. Self-assembly of CdSe-ZnS quantum dot bioconjugates using an engineered recombinant protein. J. Am. Chem. Soc. **122**: 12142–12150.
28) Medintz, I.L., Clapp, A.R., Mattoussi, H., Goldman, E.R., Fisher, B., and Mauro, J.M. 2003. Self-assembled nanoscale biosensors based on quantum dot FRET donors. Nat. Mater. **2**: 630–639.
29) Osaki, F., Kanamori, T., and Sando, S., Sera, T., and Aoyama, Y. 2004. Quantum dot conjugated sugar ball and its cellular uptake. On the size effects of endocytosis in the subviral region. J. Am. Chem. Soc. **126**: 6520–6521.
30) Pinaud, F., King, D., Moore, H.P., and Weiss, S. 2004. Bioactivation and cell targeting of semiconductor CdSe/ZnS nanocrystals with phytochelatin-related peptides. J. Am. Chem. Soc. **126**: 6115–6123.
31) Rizzuto, R., Brini, M., Pizzo, P., Murgia, M., and Pozzan, T. 1995. Chimeric green fluorescent protein as a tool for visualizing subcellular organelles in living cells. Curr. Biol. **5**: 635–642.
32) Rosenthal, S.J., Tomlinson, I., Adkins, E.M., Schroeter, S., Adams, S., Swafford, L., McBride, J., Wang, Y., DeFelice, L.J., and Blakely, R.D. 2002. Targeting cell surface receptors with ligand-conjugated nanocrystals. J. Am. Chem. Soc. **124**: 4586–4594.
33) Shibahara, A., Hoshino, A., Hanaki, K., Suzuki, K., and Yamamoto, K. 2004. On the cyto-toxicity caused by quantum dots. Microbiol. Immunol. **48**: 669–675.
34) Shubeita, G.T., Sekatskii, S.K., Dietler, G., Potapova, I., Mews, A., and Basch, T. 2003. Scanning near-field optical microscopy using semiconductor nanocrystals as a local fluorescence and fluorescence resonance energy transfer source. J. Microsc. **210**: 274–278.
35) Smith, A.M., Gao, X., and Nie, S. 2004. Quantum-dot nanocrystals for *in-vivo* molecular and cellular imaging. Photochem. Photobiol. (in press).
36) Su, X.L., and Li, Y. 2004. Quantum dot biolabeling coupled with immunomagnetic separation for detection of *Escherichia coli* O157:H7. Anal. Chem. **76**: 4806–4810.
37) Taguchi, T., Shimura, M., Osawa, Y., Suzuki, Y., Mizoguchi, I., Niino, K., Takaku, F., and Ishizaka, Y. 2004.

Nuclear trafficking of macromolecules by an oligopeptide derived from Vpr of human immunodeficiency virus type-1. Biochem. Biophys. Res. Commun. **320**: 18–26.

38) Voura, E.B., Jaiswal, J.K., Mattoussi, H., and Simon, S.M. 2004. Tracking metastatic tumor cell extravasation with quantum dot nanocrystals and fluorescence emission-scanning microscopy. Nat. Med. **10**: 993–998.

39) Wu, H.Y., Tomizawa, K., Matsushita, M., Lu, Y.F., Li, S.T., and Matsui, H. 2003. Poly-arginine-fused calpastatin peptide, a living cell membrane-permeable and specific inhibitor for calpain. Neurosci. Res. **47**: 131–135.

40) Wu, X., Liu, H., Liu, J., Haley, K.N., Treadway, J.A., Larson, J.P., Ge, N., Peale, F., and Bruchez, M.P. 2003. Immunofluorescent labeling of cancer marker Her2 and other cellular targets with semiconductor quantum dots. Nat. Biotechnol. **21**: 41–46.

41) Xu, H., Sha, M.Y., Wong, E.Y., Uphoff, J., Xu, Y., Treadway, J.A., Truong, A., O'Brien, E., Asquith, S., Stubbins, M., Spurr, N.K., Lai, E.H., and Mahoney, W. 2003. Multiplexed SNP genotyping using the Qbead system: a quantum dot-encoded microsphere-based assay. Nucleic Acids Res. **31**: 43.

NANO LETTERS

2004
Vol. 4, No. 11
2163–2169

Physicochemical Properties and Cellular Toxicity of Nanocrystal Quantum Dots Depend on Their Surface Modification

Akiyoshi Hoshino,[†,‡,§] Kouki Fujioka,[†] Taisuke Oku,[†] Masakazu Suga,[†] Yu F. Sasaki,[∥] Toshihiro Ohta,[⊥] Masato Yasuhara,[‡] Kazuo Suzuki,[§] and Kenji Yamamoto*[,†,‡]

Department of Medical Ecology and Informatics, Research Institute, International Medical Center of Japan, Toyama 1-21-1, Shinjuku, Tokyo 162-8655, Japan, Department of Pharmacokinetics and Pharmacodynamics, Hospital Pharmacy, Tokyo Medical and Dental University Graduate School, Yushima 1-5-45, Bunkyo-ku, Tokyo 113-8519, Japan, Department of Bioactive Molecules, National Institute of Infectious Diseases, Toyama 1-23-1, Shinjuku, Tokyo 162-8640, Japan, Faculty of Chemical and Biological Engineering, Hachinohe National College of Technology, Tamonoki Uwanotai 16-1, Hachinohe, Aomori 039-1192, Japan, and School of Life Science, Tokyo University of Pharmacy and Life Science, Horinouchi 1432-1, Hachioji, Tokyo 192-0392, Japan

Received August 9, 2004; Revised Manuscript Received October 5, 2004

ABSTRACT

Nanocrystal quantum dots (QDs) have been applied to molecular biology because of their greater and longer fluorescence. Here we report the potential cytotoxicity of our characterized QDs modified with various molecules. Surface modification of QDs changed their physicochemical properties. In addition, the cytotoxicity of QDs was dependent on their surface molecules. These results suggested that the properties of QDs are not related to those of QD-core materials but to molecules covering the surface of QDs.

The behavior of QDs in biological systems is not dependent on the chemical properties of surface-covered molecules but on the nanocrystal particle itself. The surface treatment of nanocrystals (surface-covered functional groups and biomolecules covering the surface of QDs) has specified the biological behavior of whole nanocrystal QDs.

With the development of nanotechnology engineering, nanomaterial products such as carbon nanotubes, fullerenes, and nanocrystal quantum dots (QDs) are now widely produced and consumed. Great quantities of those "artificial nanomaterials" have been used on the premise of being biologically and environmentally harmless, although only a few studies have reported the cellular toxicity of those materials.[1] These artificial nanomaterials are so small that they may be easily spread, stored in the environment and even in our body, and disrupt some functions of living organism consisting of complicated natural nanomaterials. It cannot be denied that these artificial nanomaterials are also detrimental, once small substances such as asbestos, coarse particulates, and particle matter exhaust from diesel engines proved to be harmful.[2–4] Thus, we need to investigate the potential toxicity of artificial nanomaterials.

QDs are now becoming widely used in biotechnology and medical applications.[5–12] QDs have several advantages over organic fluorophores with regard to high luminescence, stability against photobleaching, and a range of fluorescence wavelengths from blue to infrared depending on the particle size.[13] However, QDs aggregate easily and lose luminescence in an intracellular environment, even under acidic (pH < 5) or isotonic conditions. Therefore, it was considered difficult to replace conventional organic fluorescent probes completely with QDs.[14] Recently, some improvements were reported to prevent aggregation under intracellular conditions by the conjugation of biomolecules with QDs,[15–18] and some are used in immunohistochemical staining.[17–19] In this study, we developed several novel surface-modified QDs using carboxylic acids, polyalcohols, and amines and evaluated their physicochemical character and cytotoxicity. There are few

* Corresponding author. E-mail: backen@ri.imcj.go.jp. Tel: +81-3-3202-7181 ext 2856. Fax: +81-3-3202-7364.
† International Medical Center of Japan.
‡ Tokyo Medical and Dental University Graduate School.
§ National Institute of Infectious Diseases.
∥ Hachinohe National College of Technology.
⊥ Tokyo University of Pharmacy and Life Science.

10.1021/nl048715d CCC: $27.50
Published on Web 10/16/2004

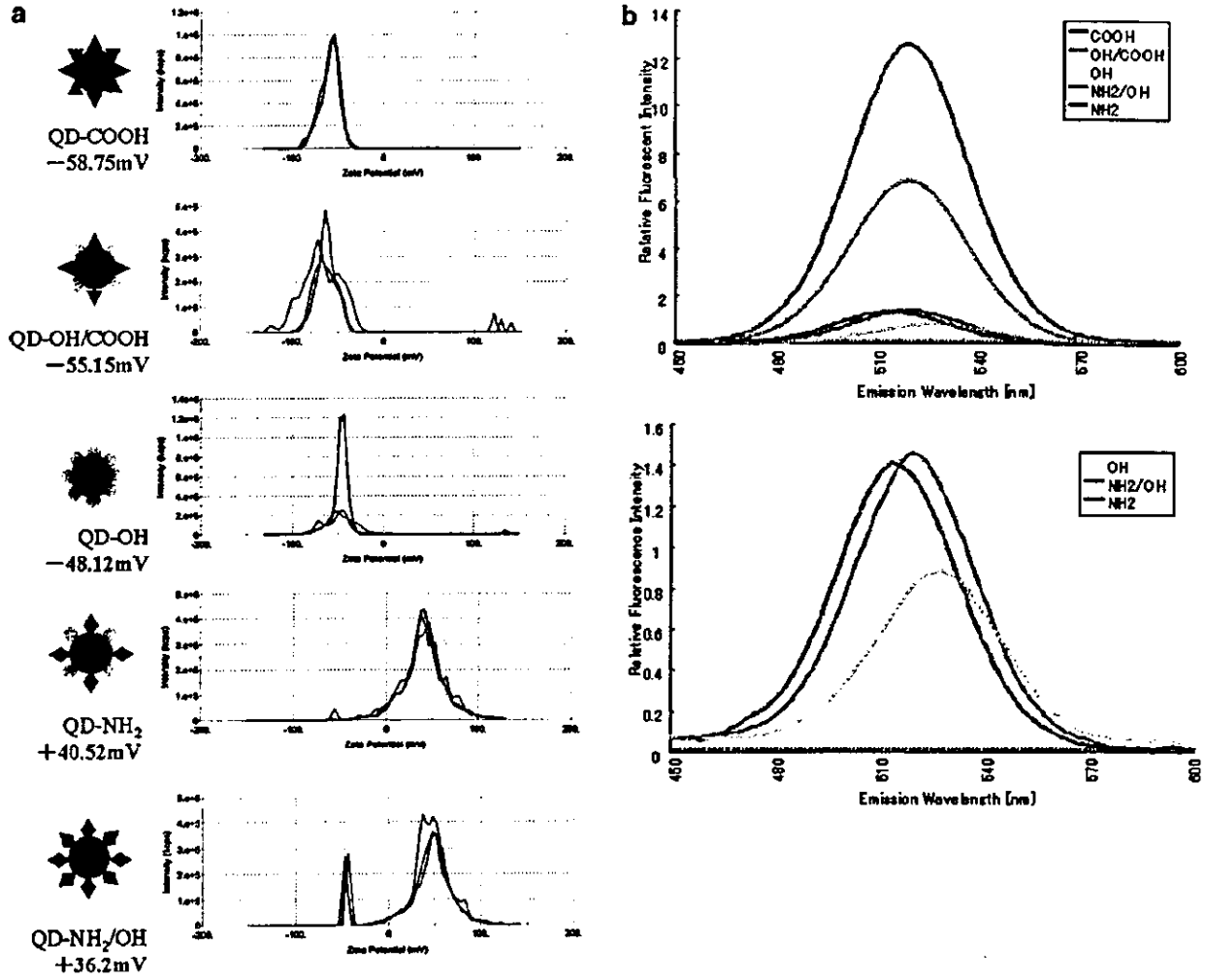

Figure 1. Surface ζ potential and fluorescence intensity of QDs varied by their surface modification. (a) Cartoon (left) and ζ potential (right) of the novel modified QDs. Surface zeta-potential of QDs is measured by electrophoresis. Each line shows the electrophoretic mobility of QDs in the stationaly layers. The data are the average of 30 assays. (b) Relative fluorescence intensity and peak wavelength of QDs measured by fluorescence spectrometry. (Lower) enlarged panel of QD-OH (yellow); QD-NH_2/OH (green) and QD-NH_2 (blue) in the upper panel. The peak emission wavelengths of QD-COOH, QD-OH/COOH, QD-OH, QD-NH_2/OH, and QD-NH_2 varied at 519, 520, 526, 520, and 513 nm, respectively.

studies on the cytotoxicity of QDs in mammalian cells, although several experiments applying to living cells and animals have already been performed.[19−25] In this study, we tested the cytotoxic potential of QDs by three different assays: comet assay, flow cytometry, and MTT assay. The comet assay, which detects DNA damage by gel electrophoresis, has been widely used to detect apoptotic cell damage induced by chemicals.[26−29] In this assay, DNA fragments can be observed as a stream from the nucleus, and the level of damage can be quantitated by the length of the stream of DNA fragments. We report here that the cytotoxicity of QDs is also caused by the surface-covering molecules of QDs but not by the nanocrystalline particle itself.

We synthesized ZnS-coated CdSe nanocrystal QDs (518-nm fluorescence peak emission). Synthesized QDs were then coated with MUA (QD-COOH), cysteamine (QD-NH_2), or thioglycerol (QD-OH) using thiol-exchange reactions as previously described.[30−32] To introduce two functional groups (QD-OH/COOH, and QD-NH_2/OH), we used equal molar quantities of thioglycerol and MUA or cysteamine and thioglycerol, respectively. To investigate the physicochemical properties of these five types of modified QDs, we measured the fluorescence intensity, particle diameter, and surface ζ potential. At first, we assessed the surface ζ potential of QDs to confirm whether the exchange reaction was performed (Figure 1a). As expected, QD-COOH and QD-OH/COOH were highly negatively charged, whereas QD-NH_2 and QD-NH_2/OH were positively charged. QD-OH was less negatively charged than the carboxylic acid groups. QDs with both hydroxyl and carboxyl/amine groups had median charge in both groups. We then assessed whether the difference in the surface modification of QDs affected the fluorescence intensity. The fluorescence intensity and peak wavelength

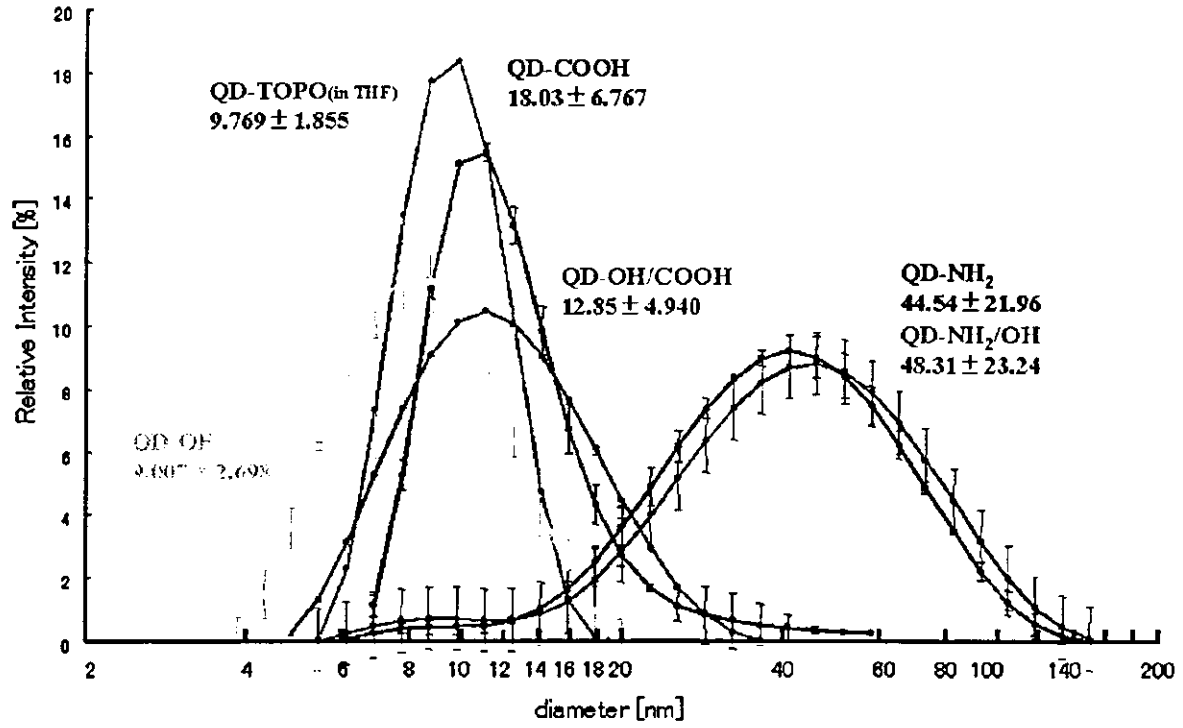

Figure 2. Size distribution of modified QDs in aqueous solution varied by their surface modification. The profile for the distribution of QDs in aqueous solution was observed by dynamic light scattering methods. Values are the mean ± standard deviation of the data measured 12 times, respectively.

were measured using a fluorescence spectrometer (Figure 1b). The QDs of carboxyl groups had higher luminescence than the other groups. Furthermore, the peak wavelength varied according to the surface modification. QDs containing amino groups emitted a shorter wavelength than the originally synthesized QD (TOPO capped-QD; 518-nm emission). In contrast, QDs with hydroxyl groups were slightly red-shifted. We assumed that a longer carbon chain and the carboxyl groups of MUA may contribute to the long lifetime and high quantum yield of QD-COOH. In contrast, the decreasing fluorescence of amino-QD particles may be caused by the oxidation of QD-metal because of the leakage of electrons from QDs through NH_2 groups in aqueous solution.[13] This suggested that the luminescence intensity of QDs may increase according to the surface-covered molecule structures.

Although it is known that the fluorescence of QDs depends on the particle size, the interparticle conformation of QDs in aqueous solution has not yet been revealed. To investigate whether any change in the particle conformation of QDs occurred in the process of surface modification, we attempted to measure the particle diameter of QDs by dynamic light scattering (DLS). We used a He−Ne laser (633-nm wavelength) light source because using a short wavelength that excites the QDs impedes the detection of QD light scattering. The size distribution of QDs was widely spread according to their modifications (Figure 2). Amino-QDs showed a broad particle distribution around 40 nm. In contrast, QDs of carboxyl groups had a narrow distribution around 20 nm. These results seemed to be contradicted by the observation that the emission wavelength of QDs depended on their particle size.[11,34] In addition, it was previously reported that transmission electron microscopy showed the diameter of the uncoated green nanocrystalline QD to be approximately 3.5 nm.[31] Positively charged amino-QDs and negatively charged impure materials in solution (such as TOPO) may form an ionic combination and affect the "apparent" diameter of the particles. In the case of carboxyl QDs, hydrophobic interaction among long carbon chains is also concerned with their larger particle distribution.

Processing the QD surface with hydroxyl group resulted in improved dispersion and stability under hypertonic conditions (Figure 3). In contrast, all of the QDs were stable in nonelectrolyte solutions. All of the modified QDs were stable for 30 min under weak alkaline conditions, whereas only QDs of the amine groups were stable under acidic conditions. These results were useful for advanced surface development to apply QDs in biological and medical fields.

To examine whether QDs affected cell proliferation, we first assessed cell proliferation by MTT assay. The reduction activity of cells was decreased by adding the crude QDs (Figure 4), but we cannot determine whether the amine-QDs were harmful because MTT reagensts were nonbiologically reduced to hormazan by the amine-QDs (data not shown). Then we determined whether this damage was caused by cell death or the suppression of cell activity. To examine whether the cell damage of QDs was affected by their surface potential, the cytotoxicity was evaluated by flow

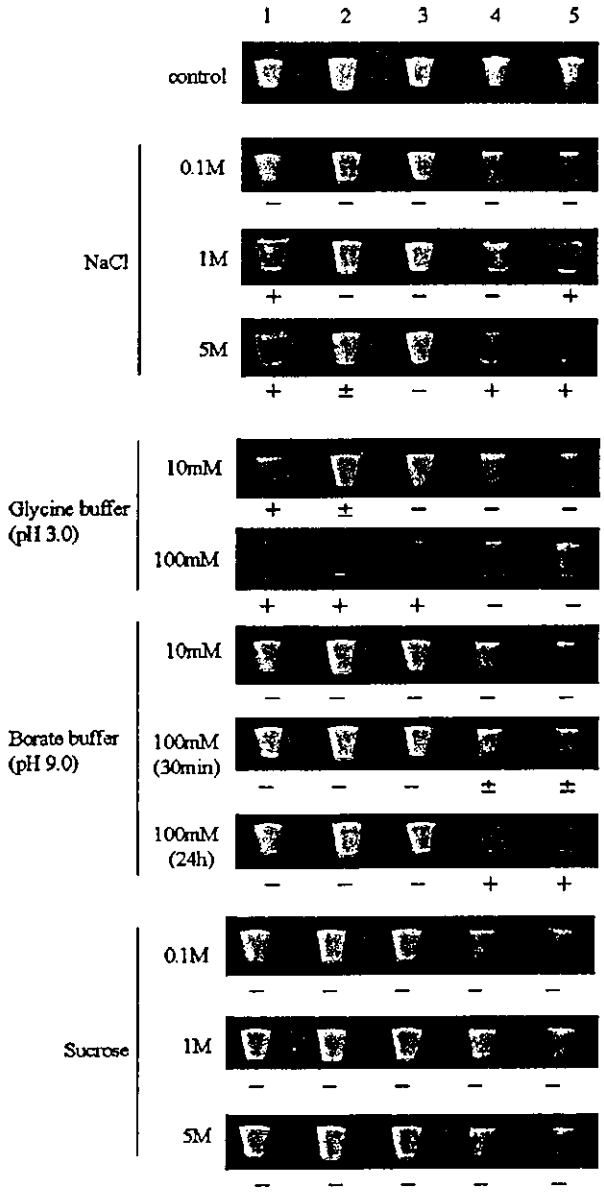

Figure 3. Physicochemical stability of various modified QDs in aqueous buffers. A QD aqueous solution (10 μM) was diluted by the indicated buffers (QD final concentration 100 nM), and incubated for 30 min at room temp. The snapshots were captured using a digital camera with $^1/_{30}$ s exposure excited by a 365-nm wavelength (UV-A). The results were reproduced in three separate experiments. 1, QD-COOH; 2, QD-OH/COOH; 3, QD-OH, 4, QD-NH_2/OH; 5, QD-NH_2; +, aggregated; ±, partially aggregated; −, not aggregated.

cytometry (Figure 5). QDs were introduced into cells by an endocytotic mechanism by adding culture media.[14,25] Cell death was observed by adding crude QDs. In contrast, low cell damage and high labeling efficiency were achieved by adding purified QDs. However, slight cell death was observed only by purified QD-COOH. This cytotoxicity may be caused by uptake QDs located in endosomes.[14] As surface molecules were bound to QDs through the electric interaction

Table 1. DNA-Damaging Effects of the Ingredients and Impurities of the QD Samples

compound	dose (μg/mL)	tail length of 50 nuclei (mm, mean ⊥ SE) 2-h treatment	12-h treatment
MUA	0	23.4 ± 1.05	23.9 ± 1.21
	25	25.6 ⊥ 0.58	28.1 ⊥ 1.31
	50	33.8 ± 2.38[a]	41.2 ± 3.31[a]
	100	54.6 ± 3.27[a]	toxic
	200	76.0 ± 3.52[a]	toxic
	400	80.3 + 3.18[a]	toxic
cysteamine	0	23.5 ⊥ 0.81	24.1 ⊥ 1.05
	50	22.4 ± 0.40	25.1 ± 1.12
	100	23.4 ± 0.95	29.6 ± 1.72
	200	22.9 ± 0.90	35.4 ± 2.89[a]
	400	23.3 ± 0.82	44.5 ± 2.21[a]
thioglycerol	0	23.5 ± 0.81	24.1 ± 1.05
	50	24.7 ± 1.06	27.0 ± 1.65
	100	26.0 ± 1.28	24.7 ± 1.24
	200	22.4 + 0.83	24.6 + 0.99
	400	23.4 ⊥ 0.98	28.1 ⊥ 1.84
TOPO	0	23.8 ± 0.91	23.1 ± 1.04
	50	24.9 ± 0.47	22.5 ± 0.56
	100	27.1 ± 1.33	26.3 ± 1.61
	200	29.6 + 1.92	28.1 + 1.33
	400	32.5 ± 1.43[a]	31.7 ± 1.31[a]
ZnS	0	23.8 ± 0.91	23.1 ± 1.04
	50	23.7 ± 0.89	24.1 ± 0.51
	100	22.5 ± 0.53	22.4 ± 0.34
	200	24.1 ⊥ 0.71	24.1 ⊥ 0.56
	400	23.3 ± 0.54	22.2 ± 0.97

[a] $P < 0.05$.

between the sulfhydryl group and QD-covered zinc,[25] surface molecules such as MUA may be detached by acidic and oxidative conditions in endosomes and released into cytoplasm.[34] The fluorescence of QDs was lost by low pH, by oxidation of the surface structures, or by some intracellular factors adsorbed onto QDs,[13] implying that the advanced development of the surface modification of QDs needs to overcome the cytotoxicity. However, this detachment could be utilized to release valuable materials such as medicines and genes into cells by cellular oxidative/reductive conditions.

Next, to investigate whether cell death by QDs was carried out by an apoptotic pathway, we evaluated the genotoxic potential of QDs by comet assay with WTK1 cells.[27-29] A significant increase in the tail length was observed after 2 h of treatment with QD-COOH at 2 μM (Figure 6a). After treatment for 12 h, the tail length was equal to that of the control cells, suggesting that the induced DNA damage was efficiently repaired during prolonged incubation. Crude QD-COOH samples prepared by only membrane filtration, but not by ultrafiltration, showed stronger DNA damage than purified QD-COOH (Figure 6b). However, QD-NH2, QD-OH, QD-OH/COOH, and QD-NH2/OH induced no DNA damage up to a dose of 4 μM for 2 h. To determine whether the genotoxicity of QDs was caused by QD particles themselves, three ingredients of the QD samples (MUA, cysteamine, and thioglycerol) and two possible impurities (TOPO and ZnS) were also assayed. As shown

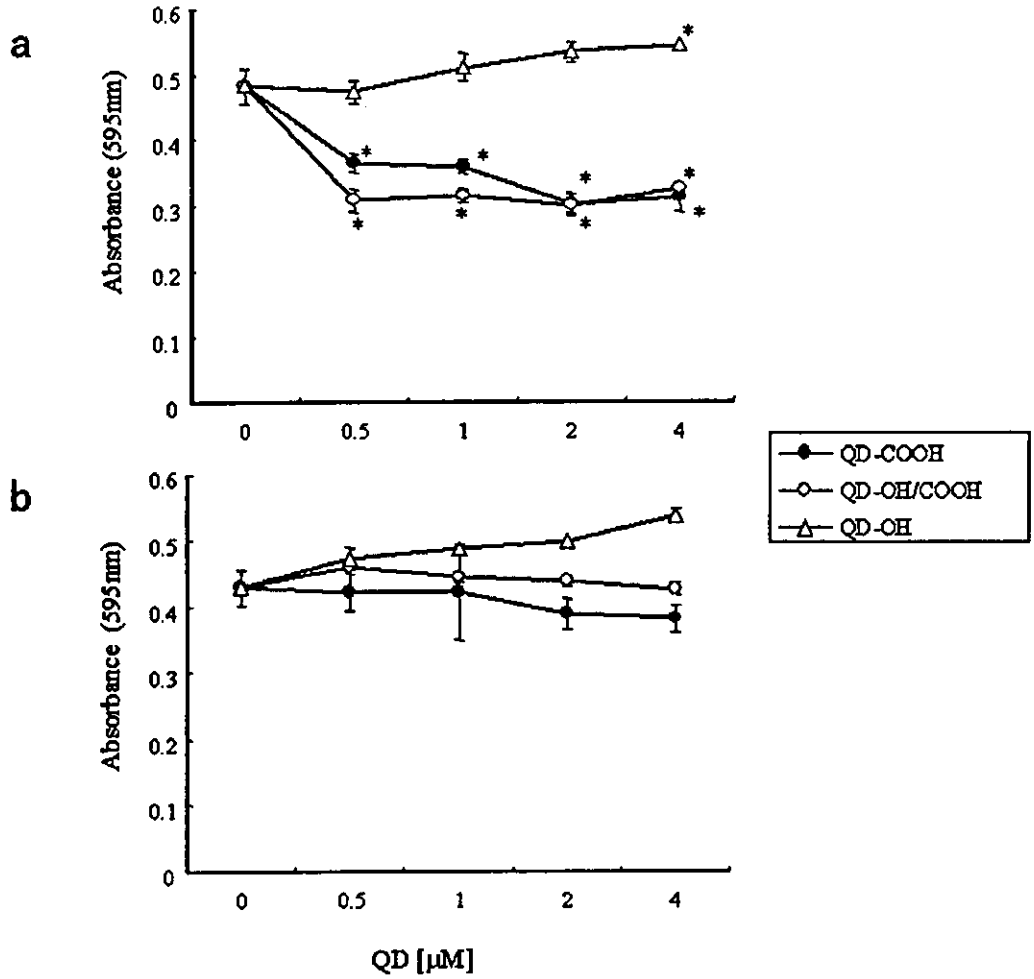

Figure 4. Contaminated impurities and ingredients in QD samples suppress the proliferation of cultured cells. Vero cells were plated at 5×10^4 cells on 96-well plates and cultured for 4 h with (a) crude QD and (b) ultrafiltartion-purified QDs in coexisting MTT reagents (Roche Diagnostics). After incubation, the cells were lysed on the plate, and 595-nm absorbance (reduced hormazan) was measured with a microplate reader. Data are presented as the mean ± standard deviation of duplicate samples. Significance was evaluated by the *t* test versus negative control. *, $p < 0.05$.

in Table 1, treatment with MUA for 12 h caused severe cytotoxicity at doses greater than 100 μg/mL (approximately coordinated to 4μM QD-COOH). DNA damage was observed at doses greater than or equal to 50 μg/mL with 2 h of treatment. Cysteamine was weakly genotoxic when cells were treated for 12 h. Thioglycerol was negative in the assay, suggesting that QD-OH was the least toxic QD among them. Because TOPO was also found to be a cytotoxic and genotoxic compound, the complete removal of TOPO from the QD samples is important in reducing toxicity. These results provided evidence that some hydrophilic compound-coated QDs are responsible for the genotoxicity of QD. Almost all of the DNA damage induced by QD-COOH was efficiently repaired in the cells because DNA damage detected by the comet assay did not persist in the cells treated for 12 h. However, the possibility remains that a few nonrepaired DNA lesions can result in gene mutations or chromosome aberrations. These results provided evidence that some hydrophilic compound-coated QDs are responsible for the cytotoxicity of QDs. It is an important factor for designing less-toxic QDs to select hydrophilic compounds to dissolve QDs in water. These results suggested that the surface treatment of nanocrystals (surface-covered functional groups and biomolecules covered the surface of QDs) has specified the biological behavior of whole nanocrystal QDs.

Nanocrystal QDs have the great potential to be applied to molecular biology and bioimaging because of several advantages over organic fluorophores. As of now, the potential toxicity of industrial products is not considered, whereas the pharmaceutical preparations cannot be commercialized without strictly investigating detrimental effect to human, resulting in the environmental pollution that was caused by the leakage of toxic substance from scrapped industrial products. We the manufacturers must be responsible for characterizing the potential environmental effects and biological toxicity of novel nanomaterial products for industrial laborers and consumers before products are widely

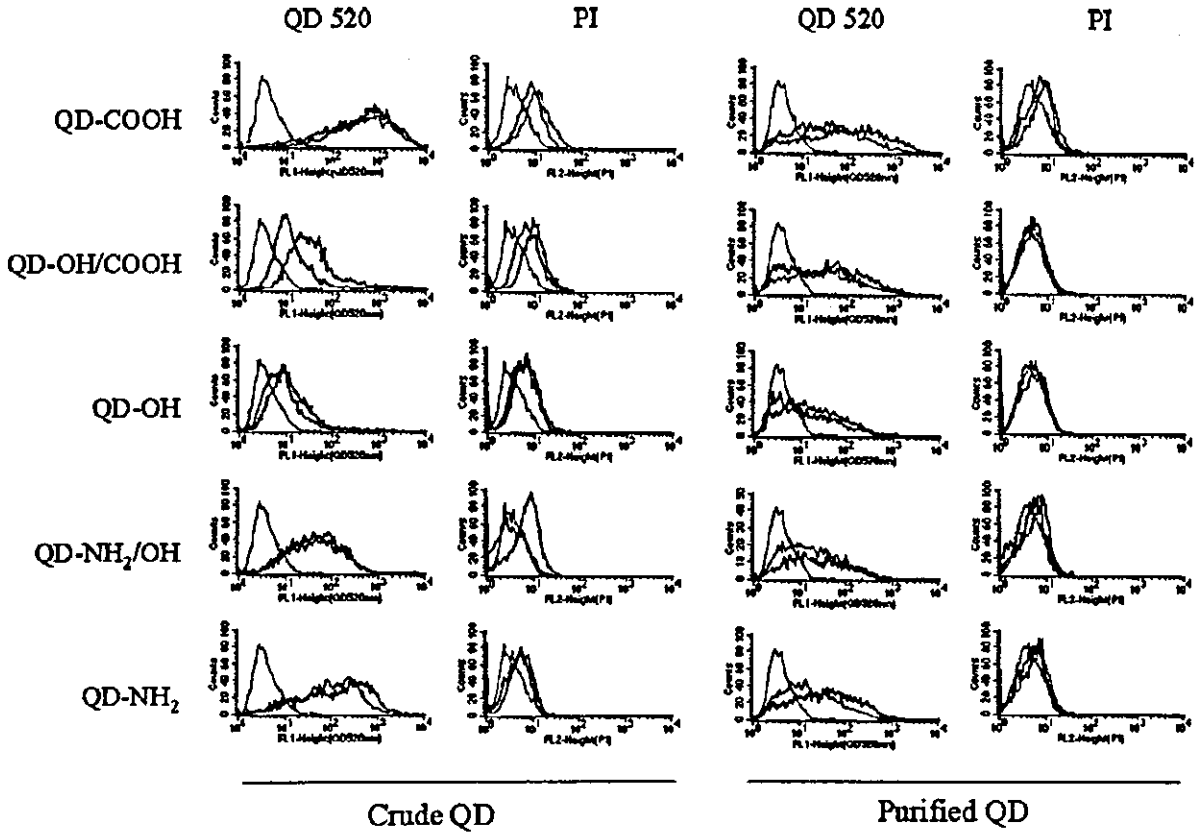

Figure 5. Contaminated impurities and ingredients in QD samples induce cell death. Vero cells were plated at 1×10^5 cells on 24-well plate and incubated for 12 h with crude QDs and ultrafiltration-purified QDs at 2 μM (red line) and 1 μM (blue line). Then cells were harvested, stained with propidium iodide, and analyzed by flow cytometry. The x axis indicates the fluorescence intensity of QDs (left columns) and PI (right columns) on a log scale. The green line shows untreated cells as a negative control. Results are representative of three separate experiments.

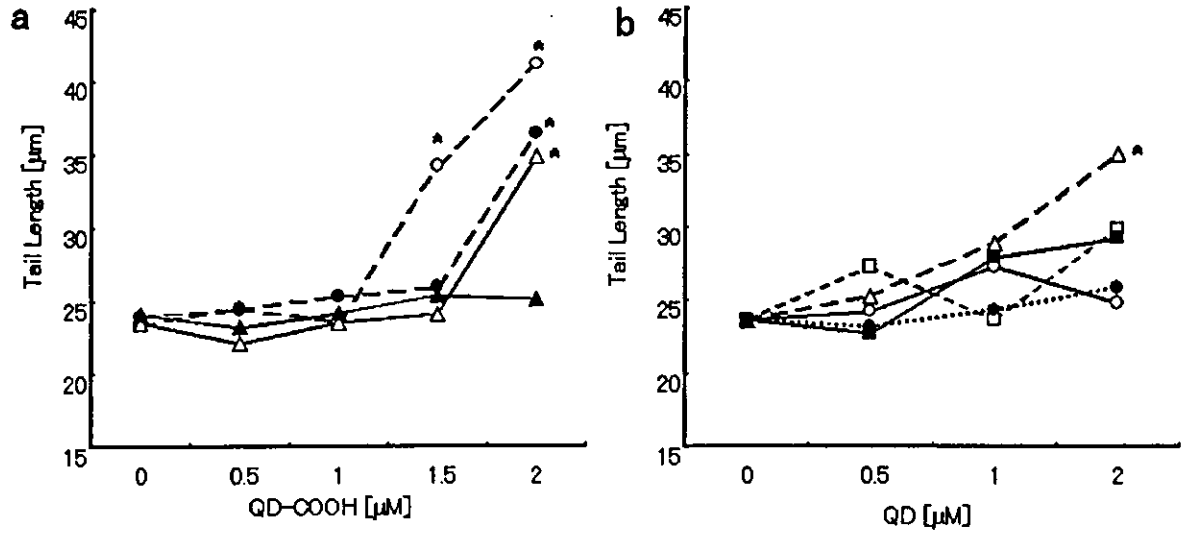

Figure 6. DNA-damaging effects of hydrophilic nanocrystalline QDs by comet assay. (a) WTK-1 cells were treated with QD-COOH (ultrafiltration purified; ▲, △) or QD-COOH (crude; ●, ○) for 2 h (open symbols) and 12 h (filled symbols). Then cells were harvested and embedded in 1% agarose, and electrophoresis was performed at 0 °C for 20 min at 25 V (0.96 V/cm) and approximately 250 mA. After being stained with ethidium bromide, the length of the whole comet was measured for 50 nuclei for each dose using a fluorescence microscope (200× magnification). (b) Cells were treated with QD-COOH (△), QD-NH_2 (□), QD-OH (○), QD-OH/COOH (●), or QD-NH_2/OH (■) for 2 h. The difference between the means in the treated and control plates was compared with the Dunnett test after one-way ANOVA. *, $p < 0.05$.

commercialized. In this paper, we revealed that the toxicity of QDs in biological systems is not dependent on the nanocrystal particle itself but on the surface molecules. In the case of QDs, no cytotoxicity was detected from their ingredients or the QD core itself, suggesting that surface processing will overcome the toxicity of nanomaterials. Less cytotoxicity derived from their ingredients or the QD core itself was observed in QD-OH in vitro. It is expected that QDs will be applied in the biomedical field for the innovative investigation, diagnosis, and medical treatment of various diseases.[9-12] When producing nanometer-sized materials in the future, it will be vital that the behavior of QDs in the biological system is not dependent on the chemical properties of surface-covered molecules but on the nanocrystalline particle itself. Surface modifications of functional molecules combined with nanoparticles may work as bionanomachines conforming to the functions designated by their surface molecules.

We conclude that the surface treatment of nanocrystals (surface-covered functional groups and biomolecules covering the surface of QDs) has specified the biological behavior of whole nanocrystalline QDs. We hope that the surface modifications of functional molecules combined with nanoparticles may work as a bionanomachine conforming to the functions designated by their surface molecules.

Acknowledgment. We are grateful to Dr. Akira Yuo and Dr. Taeko Dohi (Research Institute, IMCJ) for generously providing valuable advice about data collection. We thank Dr. Yukio Yamaguchi and colleagues (Department of Chemical System Engineering, University of Tokyo) for amino-QD improvements. This work was supported by a Medical Techniques Promotion Research Grant from the Ministry of Health, Labor and Welfare of Japan (H14-nano-004).

Supporting Information Available: Experimental procedures: Preparation of CdSe/ZnS fluorescent nanocrystal Qdots, preparation of surface-modified nanocrystal QDs, and protocols for comet assay and cell viability assays. This material is available free of charge via the Internet at http://pubs.acs.org.

References

(1) Colvin, V. L. *Nat. Biotechnol.* **2003**, *21*, 1166−1170.
(2) Borm, P. J. *Inhalation Toxicol.* **2002**, *14*, 311−324.
(3) Albrecht, C.; Borm, P. J.; Adolf, B.; Timblin, C. R.; Mossman, B. T. *Toxicol. Appl. Pharmacol.* **2002**, *184*, 37−45.
(4) Schins, R. P.; Duffin, R.; Hohr, D.; Knaapen, A. M.; Shi, T.; Weishaupt, C.; Stone, V.; Donaldson, K.; Borm, P. J. *Chem. Res. Toxicol.* **2002**, *15*, 1166−1173.
(5) Rosenthal, S. J.; Tomlinson, I.; Adkins, E. M.; Schroeter, S.; Adams, S.; Swafford, L.; McBride, J.; Wang, Y.; DeFelice, L. J.; Blakely, R. D. *J. Am. Chem. Soc.* **2002**, *124*, 4586−4594.
(6) Dubertret, B.; Skourides, P.; Norris, D. J.; Noireaux, V.; Brivanlou, A. H.; Libchaber, A. *Science* **2002**, *298*, 1759−1762.
(7) Jaiswal, J. K.; Mattoussi, H.; Mauro, J. M.; Simon, S. M. *Nat. Biotechnol.* **2003**, *21*, 47−51.
(8) Xu, H.; Sha, M. Y.; Wong, E. Y.; Uphoff, J.; Xu, Y.; Treadway, J. A.; Truong, A.; O'Brien, E.; Asquith, S.; Stubbins, M.; Spurr, N. K.; Lai, E. H.; Mahoney, W. *Nucleic Acids Res.* **2003**, *31*, 43.
(9) Wu, X.; Liu, H.; Liu, J.; Haley, K. N.; Treadway, J. A.; Larson, J. P.; Ge, N.; Peale, F.; Bruchez, M. P. *Nat. Biotechnol.* **2003**, *21*, 41−46.
(10) Chan, W. C.; Maxwell, D. J.; Gao, X.; Bailey, R. E.; Han, M.; Nie, S. *Curr. Opin. Biotechnol.* **2002**, *13*, 40−46.
(11) Zhu, L.; Ang, S.; Liu, W. T. *Appl. Environ. Microbiol.* **2004**, *70*, 597−598.
(12) Mattoussi, H.; Mauro, J. M.; Goldman, E. R.; Anderson, G. P.; Sundar, V. C.; Mikulec F. V.; Bawendi, M. G. *J. Am. Chem. Soc.* **2000**, *122*, 12142−12150.
(13) Gerion, D.; Pinaud, F.; Williams, S. C.; Parak, W. J.; Zanchet, D.; Weiss, S.; Alivisatos, A. P. *J. Phys. Chem. B* **2001**, *105*, 8861−8871.
(14) Hanaki, K.; Momo, A.; Oku, T.; Komoto, T.; Maenosono, S.; Yamaguchi, Y.; Yamamoto, K. *Biochem. Biophys. Res. Commun.* **2003**, *302*, 496−501.
(15) Medintz, I. L.; Clapp, A. R.; Mattoussi, H.; Goldman, E. R.; Fisher, B.; Mauro, J. M. *Nat. Mater.* **2003**, *9*, 630−638.
(16) Chan, W. C.; Nie, S. *Science* **1998**, *281*, 2016−2018.
(17) Goldman, E. R.; Balighian, E. D.; Mattoussi, H.; Kuno, M. K.; Mauro, J. M.; Tran, P. T.; Anderson, G. P. *J. Am. Chem. Soc.* **2002**, *124*, 6378−6382.
(18) Gao, X.; Chan, W. C.; Nie, S. *J. Biomed. Opt.* **2002**, *7*, 532−537.
(19) Akerman, M. E.; Chan, W. C.; Laakkonen, P.; Bhatia, S. N.; Ruoslahti, E. *Proc. Natl. Acad. Sci. U.S.A.* **2002**, *99*, 12617−12621.
(20) Larson, D. R.; Zipfel, W. R.; Williams, R. M.; Clark, S. W.; Bruchez, M. P.; Wise, F. W.; Webb, W. W. *Science* **2003**, *300*, 1434−1436.
(21) Mansson, A.; Sundberg, M.; Balaz, M.; Bunk, R.; Nicholls, I. A.; Onuling, P.; Tagerud, S.; Montelius, L. *Biochem. Biophys. Res. Commun.* **2004**, *314*, 529−534.
(22) Pellegrino, T.; Parak, W. J.; Boudreau, R.; LeGros, M. A.; Gerion, D.; Alivisatos, A. P.; Larabell, C. A. *Differentiation* **2003**, *71*, 542−548.
(23) Levene, M. J.; Dombeck, D. A.; Kasischke, K. A.; Molloy, R. P.; Webb, W. W. *J. Neurophysiol.* **2004**, *91*, 1908−12.
(24) Dahan, M.; Levi, S.; Luccardini, C.; Rostaing, P.; Riveau, B.; Triller, A. *Science* **2003**, *302*, 442−445.
(25) Hoshino, A.; Hanaki, K.; Suzuki, K.; Yamamoto, K. *Biochem. Biophys. Res. Commun.* **2004**, *314*, 46−53.
(26) Singh, N. P.; McCoy, M. T.; Tice, R. R.; Schneider, E. L. *Exp. Cell. Res.* **1988**, *175*, 184−191.
(27) Sasaki, Y. F.; Tsuda, S.; Izumiyama, F.; Nishidate, E. *Mutat. Res.* **1997**, *388*, 33−44.
(28) Sasaki, Y. F.; Sekihashi, K.; Izumiyama, F.; Nishidate, E.; Saga, A.; Ishida, K.; Tsuda, S. *Crit. Rev. Toxicol.* **2000**, *30*, 629−799.
(29) Tice, R. R.; Agurell, E.; Anderson, D.; Burlinson, B.; Hartmann, A.; Kobayashi, H.; Miyamae, Y.; Rojas, E.; Ryu, J. C.; Sasaki, Y. F. *Environ. Mol. Mutagen.* **2000**, *35*, 206−221.
(30) Hines, M. A.; Guyot-Sionnest, P. *J. Phys. Chem.* **1996**, *100*, 468−471.
(31) Dabboussi, B. O.; Rodriguez-Viejo, J.; Mikulec, F. V.; Heine, J. R.; Mattoussi, H.; Ober, R.; Jensen, K. F.; Bawendi, M. G. *J. Phys. Chem. B* **1997**, *101*, 9463−9475.
(32) Reynolds, C. P.; Biedler, J. L.; Spengler, B. A.; Reynolds, D. A.; Ross, R. A.; Frenkel, E. P. *J. Natl Cancer Inst.* **1986**, *76*, 375−87.
(33) Liber, H. L.; Yandell, D. W.; Little, J. B. *Mutat. Res.* **1989**, *216*, 9−17.
(34) Bruchez, M., Jr.; Moronne, M.; Gin, P.; Weiss, S.; Alivisatos, A. P. *Science* **1998**, *281*, 2013−2016.

NL048715D

IMMUNOPHARMACOLOGY AND IMMUNOTOXICOLOGY
Vol. 26, No. 4, pp. 527–543, 2004

Induction of Coronary Arteritis with Administration of CAWS (*Candida albicans* Water-Soluble Fraction) Depending on Mouse Strains

Noriko Nagi-Miura,[1] Yuko Shingo,[1] Yoshiyuki Adachi,[1] Akiko Ishida-Okawara,[2] Toshiaki Oharaseki,[3] Kei Takahashi,[3] Shiro Naoe,[3] Kazuo Suzuki,[2] and Naohito Ohno, Ph.D.[1,*]

[1]Laboratory for Immunopharmacology of Microbial Products, School of Pharmacy, Tokyo University of Pharmacy and Life Science, Hachioji, Tokyo, Japan
[2]Department of Bioactive Molecules, National Institute of Infectious Diseases, Tokyo, Japan
[3]Department of Pathology, Ohashi Hospital, Toho University School of Medicine, Tokyo, Japan

ABSTRACT

The intraperitoneal administration of CAWS (water-soluble extracellular polysaccharide fraction obtained from the culture supernatant of *Candida albicans*) to mice induces coronaritis similar to Kawasaki disease. We analyzed differences in the production of cytokines involved in the occurrence of coronary arteritis among mouse strains, C3H/HeN, C57BL/6, DBA/2 and CBA/J that were injected with CAWS at 4 mg/mouse for 5 consecutive days in the first week and the fifth week of administration. The incidence of arteritis was 100% in C57BL/6, C3H/HeN and DBA/2 mice, but only 10% in CBA/J mice. The coronary arteritis observed in DBA/2 mice

*Correspondence: Prof. Naohito Ohno, Ph.D., Laboratory for Immunopharmacology of Microbial Products, School of Pharmacy, Tokyo University of Pharmacy and Life Science, 1432-1, Horinouchi, Hachioji, Tokyo 192-0392, Japan; Fax: 81-426-76-5570; E-mail: ohnonao@ps.toyaku.ac.jp.

DOI: 10.1081/IPH-200042295
0892-3973 (Print); 1532-2513 (Online)

was the most serious, with several mice expiring during the observation period. The CAWS-sensitive strains revealed increased levels of IL-6 and IFN-γ during the course of a specific response to CAWS by spleen cells. In contrast, IL-10 levels were observed to increase markedly in CAWS-resistant CBA/J mice, but not the CAWS-sensitive strains. However, TNF-α levels were more elevated only in DBA/2 mice. The difference in disease development and cytokine production strongly suggests that the genetic background of the immune response to CAWS contributes to the occurrence of coronary arteritis.

Key Words: *Candida albicans*; Induction of arteritis; Polysaccharide; DBA/2 mice.

INTRODUCTION

Kawasaki disease, also referred to as acute febrile mucocutaneous lymph node syndrome or MCLS, was first reported by Kawasaki in 1967.[1,2] A disease of unknown cause, it affects mainly children aged 4 and under. The number of patients diagnosed with Kawasaki disease annually is roughly 10,000. The patients present with systemic coronary arteritis, and the greatest concern with this symptom is the occurrence of coronary arteritis or coronaritis, which occurs as a sequela in nearly 10% of all patients.[3,4] Moreover, in the case of the formation of giant coronary aneurysms, complications involving myocardial ischemia and myocardial disorders caused by vascular occlusion due to thrombus formation may arise. In actuality, sudden death due to myocardial infarction occurs in several percent of Kawasaki disease patients. Although the occurrence of such coronary artery disorders has decreased with the introduction of γ-globulin therapy, the mechanism of their occurrence along with the pharmacological mechanism of the treatment is unknown.[5,6]

Murata et al.[7,8] reported that Kawasaki-disease-like coronary arteritis was induced specifically at the origin of the coronary arteries in mice administered an alkaline extract of *C. albicans* isolated from patients (CADS) with Kawasaki disease. Ishida-Okawara et al.[9] have demonstrated that mice with coronary arthritis induced with a CADS injection show an increase in anti-myeloperoxidase (MPO)-specific anti-neutrophil cytoplasmic antibody (MPO-ANCA) in their serum. In addition, MPO was identified to be the antigen to MPO-ANCA using MPO-deficient mice.[9] These findings show the substances including β-glucan derived from *C. albicans* might relate to coronary arteritis.

The number of opportunistic infections is on the rise accompanying the proliferation of highly advanced medical treatment. *Candida* infections are frequently observed in patients in high-risk groups.[10,11] As the chemotherapeutic agent for mycoses is completely different from that for bacterial infections, early diagnosis is critical.[12,13] Since fungal cell wall contains β-glucan as its main component, β-glucan is detected in the blood of patients with deep mycoses. Thus, measurement of β-glucan in the blood is widely used for the early diagnosis of deep mycoses.[14,15] In this study, we cultured *Candida* spp. in completely synthetic media, obtained the water-soluble polysaccharide fraction released into the culture supernatant (*Candida albicans* water-soluble fraction or CAWS), and performed various analyses on that fraction. As a result, CAWS was found to be composed of mannoprotein and a β-glucan complex and to activate the limulus G factor, to exhibit acute lethal toxicity in the case of

intravenous administration, and to activate vascular endothelial cells, platelets and lymphocytes.[16-18] In addition to CADS, other substances in the soluble fraction may cause the development of coronary arteritis in mice.

In the present study, the incidence of coronaritis was found to be higher when CAWS was administered than when the conventional alkaline extract was administered, and a difference in the incidence was observed among mouse strains. We also analyzed the correlation of cytokine production in the development of coronary arteritis induced by CAWS.

MATERIALS AND METHODS

Mice

Male C3H/HeN and DBA/2 mice were purchased from Japan SLC, whereas male C57BL/6 and CBA/J mice were purchased from Charles River Japan. The mice were housed in a specific pathogen-free (SPF) environment and were used in the study at 5–14 weeks of age.

Organisms

Candida albicans strain IFO1385 was purchased from the Institute for Fermentation, Osaka (IFO), stored at 25°C on Sabauroud's agar (Difco, USA) and passaged once every three months.

Preparation of CAWS

CAWS was prepared from *C. albicans* strain IFO1385 in accordance with conventional methods.[18] The procedure used is as follows: 5 L of medium (C-limiting medium) was added to a glass incubator and cultured for 2 days at 27°C while supplying air at a rate of 5 L/min and rotating at 400 rpm. Following the culture, an equal volume of ethanol was added and after the mixture was allowed to stand overnight, the precipitate was collected. The precipitate was dissolved in 250 mL of distilled water, ethanol was added and the mixture was allowed to stand overnight. The precipitate was collected and dried with acetone to obtain CAWS.

Administration Schedule for Induction of Coronary Arteritis

CAWS (0 or 4 mg/mouse) was administered intraperitoneally for 5 consecutive days to each mouse in week 1. In week 5, CAWS (0 or 4 mg/mouse) was again administered in the same manner as that in week 1, after which the mice were sacrificed in week 9. The hearts of the animals were fixed with 10% neutral formalin and prepared in paraffin blocks. Tissue sections were stained with Hemotoxylin-Eosin (HE) stain. Cells were prepared from the spleen and cultured. Cells were also prepared from peritoneal exudative cells (PECs) and from the thymus, and enumerated. Liver weight was measured.

Preparation of Mouse Serum

The mice were anesthetized with chloroform and then sacrificed after which blood was drawn from the heart. After the blood samples had been left to stand for 60 minutes at room temperature and then for 60 minutes at 4°C, they were separated by centrifugation at 15,000 rpm × 10 minute, and the resulting supernatant was used as the serum. All the samples were stored at −25°C or lower.

CAWS-Specific Reaction in the Isolated Spleen Cells

The mice were anesthetized and then sacrificed, after which the spleen was excised. After teasing using a mesh in RPMI-1640 medium, the tissue was separated by centrifugation at 1200 rpm × 5 minute, and the resulting cells were treated with ACK-lysing buffer (NH_4Cl 8.20 g/L, $KHCO_3$ 1 g/L, EDTA·2Na 37.2 mg/L). After two washes with RPMI medium, the spleen cells were counted to adjust the cell density and then used after being suspended in RPMI medium with 10% FCS (fetal calf serum). The spleen cells were adjusted to 1×10^7 in RPMI 1640 medium containing 10% FCS and 500 µl aliquots were added to each well of a 48-well plate. Following the addition of CAWS (0, 2.5, 5 or 10 µg/ml), the cells were culture for 48 hours in a 5% CO_2 incubator at 37°C. The cytokine level of the culture supernatant was determined by Enzyme-Linked Immuno Sorbent Assay (ELISA) as described below.

Measurement of IL-1β, IL-4, IL-10 and IL-12

The IL-1β level was measured using a Mouse IL-1β ELISA Kit (Biosource International). Levels of IL-4, IL-10 and IL-12 were measured using Mouse IL-4, IL-10 and IL-12 $O_{PT}EIA^{TM}$ Kits (Pharmingen).

Measurement of IL-6

An ELISA 96-well plate (Sumitomo Bakelite) was coated with rat anti-mouse IL-6 mAb (Pharmingen) using 0.1 M bicarbonate buffer (pH 9.5) and incubated overnight at 4°C. After a wash with Phosphate buffered saline with 0.05% Tween 20 (PBST), the antibody was blocked for 40 minutes at 37°C with BPBST. This was followed by the addition of standard and sample (50 µL), incubation for 40 minutes at 37°C and washing with PBST. Fifty microliters of a secondary antibody in the form of biotinylated rat anti-mouse IL-6 mAb (1/2000; Pharmingen) was then added, and after incubation for 40 minutes at 37°C and a wash with PBST, peroxidase-conjugated streptavidin (1/10000; Zymed Laboratories, Inc.) was added. This was followed by incubation for 40 minutes at 37°C and washing with PBST. Subsequently, 50 µL of peroxidase substrate (TMB microwell peroxidase substrate system, KPL Inc.) was added to generate color, and absorbance was measured as previously described. Recombinant mouse IL-6 (Pharmingen) was used as the standard.

Measurement of IFN-γ

An ELISA 96-well plate (Sumitomo Bakelite) was coated with rat anti-mouse IFN-γ monoclonal antibody (mAb; Pharmingen) using 0.1 M $NaHCO_3$ (pH 8.2) and

incubated overnight at 4°C. After a wash with 0.05% Tween-PBS (PBST), the antibody was blocked for 40 minutes at 37°C with 0.5% BSA (bovine serum albumin)-PBST (BPBST). This was followed by the addition of standard and sample (50 μL), incubation for 40 minutes at 37°C and washing with PBST. Fifty microliters of a secondary antibody in the form of biotinylated rat anti-mouse IFN-γ (1/1000; Pharmingen) was then added, and after incubation for 40 minutes at 37°C and a wash with PBST, peroxidase-conjugated streptavidin (1/2000; Pharmingen) was added. This was followed by incubation for 40 minutes at 37°C and washing with PBST. Subsequently, color was generated using peroxidase substrate (TMB microwell peroxidase substrate system, KPL Inc.). After termination of the reaction with 1 M phosphoric acid, absorbance (OD 450/Ref. 630) was measured. Recombinant mouse IFN-γ (Pharmingen) was used as the standard.

Measurement of TNF-α

An ELISA 96-well plate (Nunc) was coated with rat anti-mouse TNF-α mAb (1/500; Pharmingen) using 0.1 M NaH_2PO_4– 0.1 M Na_2HPO_4 buffer (pH 6.0) and incubated overnight at 4°C. After a wash with PBST, the antibody was blocked for 60 minutes at room temperature with BPBST. This was followed by the addition of standard and sample (50 μL), incubation for 3 hours at room temperature and washing with PBST. Fifty microliters of a secondary antibody in the form of biotinylated rat anti-mouse TNF-α mAb (1/1000; Pharmingen) was then added, and after incubation for 60 minutes at room temperature and a wash with PBST, horseradish-peroxidase-conjugated streptavidin (1/1000; Pharmingen) was added. This was followed by incubation for 30 minutes at room temperature and washing with PBST. Subsequently, color was generated and absorbance was measured as previously described. Recombinant mouse TNF-α (Pharmingen) was used as the standard.

Measurement of Anti-CAWS Antibody Titer

An ELISA 96-well plate (Nunc) was coated with CAWS using 0.1 M bicarbonate buffer (pH 9.5) and incubated overnight at 4°C. After a wash with PBST, the antibody was blocked for 60 minutes at 37°C with BPBST and again washed with BPST. A serum sample diluted with BPBST (50 μl) was added, and incubation continued for another 60 minutes at 37°C. After a wash with PBST, 50 μL of peroxidase-conjugated goat anti-mouse IgG + IgM Ab (1/5000; Wako) was added and reaction was allowed to proceed for 60 minutes at 37°C. Color was generated and absorbance was measured as previously described. Furthermore, color generation was stopped after 10 minutes.

Measurement of Antibody Subclass

An ELISA 96-well plate (Nunc) was coated with CAWS using 0.1 M bicarbonate buffer (pH 9.5) and incubated overnight at 4°C. After a wash with PBST, the antibody was blocked for 60 minutes at 37°C with BPBST and again washed with PBST. A serum sample (50 μL) diluted with BPBST was added and incubation continued

for another 60 minutes at 37°C. After a wash with PBST, 50 μL of biotin-conjugated anti-mouse IgG1 (1/1000)-IgG2a (1/3000)-IgM (1/5000) Ab or peroxidase-conjugated anti-mouse IgE Ab (1/500) was added and the reaction was allowed to proceed for 60 minutes at 37°C. With respect to the biotin-conjugated antibody, after a wash with PBST, horseradish-peroxidase-conjugated streptavidin (1/5000; Pharmingen) was added, and incubation was continued for 60 minutes at 37°C. Color was generated and absorbance measured as previously described. Furthermore, color generation was stopped after 10 minutes.

Test for Significant Difference

Tests for significant differences in this study were performed using Student's t-test and values of $P<0.05$ were judged significant.

RESULTS

Development of Coronary Arteritis Induced with CAWS and Difference Among Strains

Administration of CAWS induced the development of coronary arteritis (Fig. 1). The arteritis-inducing activity of CAWS was compared among four mouse strains in accordance with the method of Murata et. al.[7,8] CAWS was dissolved in physiological saline to a concentration of 4 mg/0.2 mL, administered intraperitoneally to each mouse for five consecutive days, and again administered for five consecutive days in week 5, after which the mice were sacrificed in week 9. The tissue sections in the ninth week were prepared from the origin of the coronary arteries of the coronary aorta and stained with HE. The coronary arteritis induced by CAWS was accompanied by hypertrophy of the tunica intima, the rupture of elastic fibers and a diffuse invasion by lymphocytes, histiocytes, fibroblasts, smooth muscle cells and eosinophils of vascular endothelial cells and the regions surrounding blood vessels (Fig. 1). On the basis of such characteristics, the coronary arteritis induced by CAWS was presumed to be the so-called proliferative granulomatous coronary arteritis, and is clearly different from fibrinoid arteritis. Differences in the incidence of coronary arteritis were observed among the mouse strains. The coronary arteritis was observed in all mice of the DBA/2, C57BL/6 and C3H/HeN strains. It was observed to cover nearly the entire periphery of the vessels in DBA/2 mice, and those mice were considered to demonstrate the most virulent form of coronary arteritis (data not shown). On the other hand, CBA/J mice exhibited the lowest incidence of coronary arteritis among the four strains tested (10%), with few sites where coronary arteritis occurred.

Comparison of Survival Rates Among CAWS-Administered Mice

Among the mice administered CAWS according to the coronary arteritis induction protocol, only DBA/2 mice exhibited high mortality. Therefore, the disease

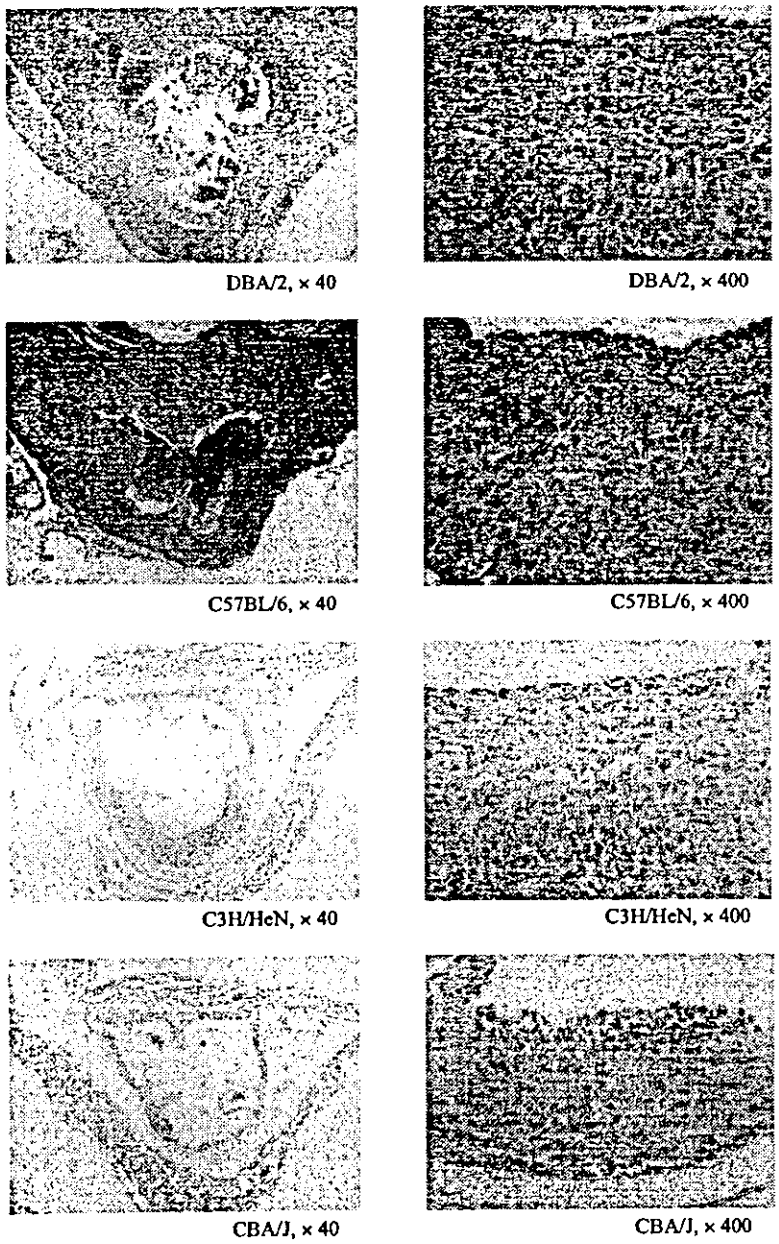

Figure 1. Histological observations of coronary arteritis. CAWS (4 mg/mouse) was administered i.p. to DBA/2, C57BL/6, C3H/HeN and CBA/J mice for five consecutive days in the 1st and 5th week. In the 9th week, mice were sacrificed and prepared sections stained with the hematoxylin-eosin method.

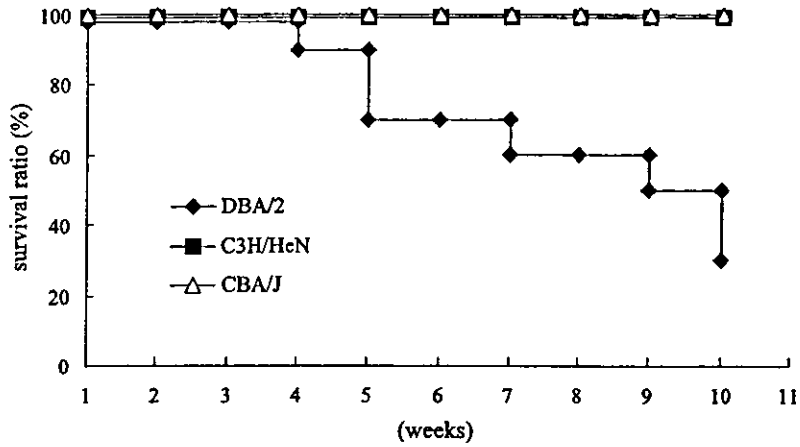

Figure 2. Survival ratio of CAWS-administered mice. CAWS (4 mg/mouse) was administered i.p. to DBA/2, C3H/HeN and CBA/J mice for five consecutive days in the 1st and 5th week. Survival had been observed for ten weeks. (N = 10).

course was examined in DBA/2 mice. DBA/2 mice were confirmed to expire beginning in the fourth week after the start of administration. The number that expired gradually increased and by the ninth week when the mice were assessed for coronary arteritis, the survival rate had dropped to 50%, and ultimately decreased to 30% (Fig. 2).

Tissue sections were prepared from the hearts of expired DBA/2 mice and observed microscopically using the HE stain. In the DBA/2 mice that expired due to administration of CAWS (n = 3), prominent neutrophil and histiocyte invasion was observed, along with the disappearance of striated muscle (Fig. 3A), and in some of the tissue, fibrosis appeared to occur in addition to cellular invasion (Fig. 3B and C); namely, the cause of death was suggested to be myocardial infarction. On the basis of these findings, it was suggested that the most virulent form of coronary arteritis was induced in DBA/2 mice, which resulted in the occurrence of cardiac ischemia that ultimately led to myocardial infarction.

Change of Cell Number in Organs on CAWS-Administration

As we observed a high incidence of cornory arteritis induced with CAWS in three strains, the increase in the numbers of immune cells was determined, along with the weight of the liver. These measurements were made in mice administered CAWS in accordance with the coronary arteritis induction protocol. In the spleen, although splenomegaly was observed in C3H/HeN, DBA/2 and C57BL/6 mice, significant increases in cell counts were exhibited by only C3H/HeN and DBA/2 mice (Fig. 4A). There were no changes in the thymus cell count in any mouse strains (Fig. 4B). In the case of PECs, although the changes were not significant, all strains exhibited an increase (Fig. 4C). There were no changes in liver weight (Fig. 4D).